

XVI. PLASMA MAGNETOHYDRODYNAMICS AND ENERGY CONVERSION*

Prof. G. A. Brown	M. T. Badrawi	G. B. Kliman
Prof. E. N. Carabateas	J. L. Coggins	A. G. F. Kniazzezh
Prof. R. S. Cooper	R. K. Edwards	B. T. Lubin
Prof. W. H. Heiser	J. R. Ellis, Jr.	C. A. McNary
Prof. W. D. Jackson	J. W. Gadzuk	R. P. Porter
Prof. J. L. Kerrebrock	T. K. Gustafson	C. V. Smith
Prof. A. H. Shapiro	J. B. Heywood	A. Solbes
Prof. R. E. Stickney	R. W. King	R. J. Thome
Dr. E. S. Pierson		J. C. Wissmiller

RESEARCH OBJECTIVES AND SUMMARY OF RESEARCH

1. Magnetohydrodynamics

Our work in magnetohydrodynamics is broadly concerned with the interactions between electromagnetic fields and electrically conducting fluids, particularly in those situations to which a continuum fluid description is applicable. Both plasmas and liquid metals are employed in the experimental aspects of our work and the development of measurement techniques receives particular attention.

(a) Plasma Magnetohydrodynamics

The goals of this research are to improve the capabilities of the magnetic annular shock tube for producing quantities of uniform, shock-heated gas, and to investigate means for measuring relevant physical properties of the shock-heated gas.

Recent experiments have shown that, although the azimuthal uniformity and the shot-to-shot reproducibility of all observed quantities are extremely high, the amount of uniform, shock-heated gas is much less than anticipated. During the coming year we shall attempt to increase the amount of uniform, shock-heated gas produced in any experiment. In particular, modifications of the magnetic annular shock tube will be made (for example, stronger preionization) to test those solutions to the problem suggested by experience, and new instrumentation will be sought (for example, to measure temperature) to help explain the loss of uniform, shock-heated gas.

The magnetic annular shock tube is also useful for the study of complex magnetohydrodynamic shock waves. A series of careful experiments near the "switch-on" shock point will be performed in an attempt to resolve several unsettled basic questions regarding the nature of the shocks that may exist there.

W. H. Heiser, J. B. Heywood

(b) Magnetohydrodynamic Wave Phenomena

One of our experiments is concerned with the excitation of Alfvén waves in a liquid metal (NaK alloy). Generation of these waves by using a current-sheet excitation has been verified, and shown to be markedly superior to the mechanical methods used in experiments reported previously. The systematic study of the excitation transmission, attenuation, and reflection of these waves in the hydromagnetic waveguide continues.

A second waveguide study is concerned with MHD wave propagation in nonuniform magnetic fields. NaK alloy again serves as the working fluid for the experimental part of this investigation.

* This work was supported in part by the U. S. Air Force (Aeronautical Systems Division) under Contract AF33 (615)-1083 with the Air Force Aero Propulsion Laboratory, Wright-Patterson Air Force Base, Ohio; and in part by the National Science Foundation (Grant GK-57).

(XVI. PLASMA MAGNETOHYDRODYNAMICS)

A theoretical study of MHD surface waves on fluids of finite electrical conductivity is also being undertaken. An experimental study of some aspects of these waves has recently been initiated, and will also use NaK as the working fluid.

W. D. Jackson

(c) Magnetohydrodynamic Channel Flow and Turbulence

The flow characteristics of electrically conducting fluids in channels or ducts are of interest in connection with many engineering applications of magnetohydrodynamics. While these include both liquid and ionized gas flows, the use of liquid metals has advantages for a considerable range of laboratory investigations.

A closed-loop flow facility has been constructed with NaK used as the working fluid. This loop is being used for study of pressure drop versus flow-rate relations (including those for MHD power-conversion devices), and the characteristics of turbulence in the presence of magnetic fields.

The character of MHD turbulence is modified when a pronounced Hall effect occurs in the flow. The characteristics of turbulence in this situation are being investigated, and work continues on the application of Norbert Wiener's "Calculus of Random Functionals" to the study of turbulent-flow situations.

W. D. Jackson

(d) Ionization Waves in Weakly Ionized Plasmas

Experiments dealing with the interaction of sonic waves propagating in the neutral background of a weakly ionized gas with induced ionization waves are now under way. Some recent observations of this phenomenon indicate that the interaction is quite strong and may provide a technique for sound-wave or ionization-wave amplification.

Two models have been developed for the ionization, either of which could describe the processes responsible for the ionization-wave propagation and the sound-wave interaction. These models will be tested against experimental results.

R. S. Cooper

2. Energy Conversion

Our studies include both magnetohydrodynamic and thermionic methods of generating electrical power, and involve over-all system considerations, properties of working fluids, and operating characteristics of conversion devices.

(a) Magnetohydrodynamic Power Generation with Liquid Metals

The generation of electrical power in space vehicles offers a potential application for MHD generators to operate on a closed-cycle system in which a nuclear reactor is the thermal-energy source. An important feature of an MHD system is the absence of rotating parts, and, to utilize it, a working fluid is required with a sufficiently high electrical conductivity at the temperatures involved. A scheme in which a liquid metal is used as the working fluid in the MHD generator duct is under investigation. Kinetic energy is imparted to this flow by driving it with its own vapor in a condensing-ejector system.

During the coming year studies will be completed on the system described in Quarterly Progress Report No. 72 (pages 155-156). These studies will include a weight analysis for a 300 KWe system. Since the condensing ejector performance has been identified as a critical element in the system, detailed analytical and experimental studies will be made on the device. The analytical studies involve the development of a theoretical model for the mixing processes in the mixing section of the condensing ejector. The experimental studies will utilize steam-water flows to verify the predictions of the

(XVI. PLASMA MAGNETOHYDRODYNAMICS)

mixing section analysis. Experimental conditions will be selected to correspond to high-performance operation of the condensing ejector.

G. A. Brown, W. D. Jackson

(b) Magnetohydrodynamic Induction Generator

The MHD induction machine utilizes the interaction between a traveling magnetic field (such as that produced by a polyphase winding) and a channeled, flowing fluid that may be either a plasma or a liquid metal.

The theory will be extended and refined during the coming year to include further studies on the design and feasibility of the induction generator for liquid-metal flows. An improved experimental model is now under construction to provide comparison with the theoretical predictions.

W. D. Jackson, E. S. Pierson

(c) Alkali-Metal Generators

Our principal objective is still to assess the feasibility of operating an MHD generator with pure alkali-metal vapor at temperatures between 1500°K and 2000°K. The work thus far indicates that the vapor will have to be dry. Our next series of experiments will be directed toward more detailed study of the dry vapor.

It has become clear, also, that the study of a wet nonequilibrium vapor is a useful method for diagnostics of condensation, and our future work will explore this possibility.

J. L. Kerrebrock

(d) Thermionic Energy Conversion

The maximum efficiency and power output of thermionic converters are limited, at present, by the conflicting requirements of obtaining high thermionic currents, reasonable output voltages, and sufficient ionization to reduce space charge. Our objective is to investigate the surface and plasma problems that most strongly influence converter performance.

Studies of the thermionic properties of cesium-covered monocrystalline and polycrystalline surfaces of refractory metals will be extended, both experimentally and analytically. The possible beneficial effects of additives (for example, oxygen and fluorine) will be considered.

The mechanisms of volume ionization in thermionic converters are being investigated. This work, together with planned spectroscopic studies, is directed toward developing a more accurate interpretation of converter performance characteristics.

E. N. Carabateas, R. E. Stickney

A. VELOCITY PROFILES FOR MAGNETOHYDRODYNAMIC FLOWS IN RECTANGULAR DUCTS

The influence of a uniform magnetic field on the steady laminar flow of a conducting fluid between two parallel infinite insulating plates was analytically described, in 1937, by Hartmann¹ for the case in which the magnetic field is perpendicular to the plates. Since that time, analytical solutions have been found for flows in rectangular ducts.²⁻⁴

The detailed character of these results in the form of velocity and induced-current profile is given here.

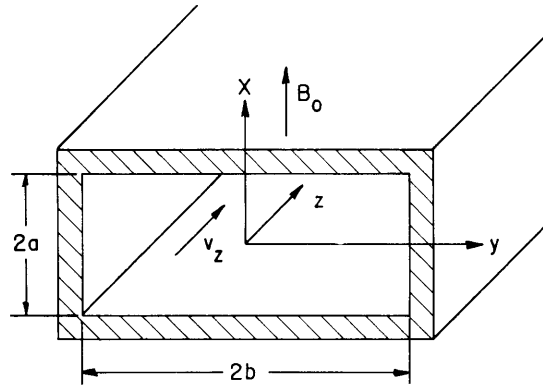


Fig. XVI-1. Channel-flow geometry.

The channel geometry is shown in Fig. XVI-1. The walls of the channel are rigid so that the fluid occupies an area between $x = \pm a$ and $y = \pm b$ and is constrained to move in the z direction. The aspect ratio $\ell = b/a$ is a significant parameter in the solutions. There is a uniform applied magnetic field B_0 in the x direction, and the significant parameter associated with this quantity is the magnetic Hartmann number

$$M = B_0 a \sqrt{\frac{\sigma}{\eta}},$$

where σ is the conductivity, and η is the dynamic viscosity of the fluid.

The equations relating the fluid velocity and other field variables are the Navier-Stokes equation, which includes the $\bar{\mathbf{J}} \times \bar{\mathbf{B}}$ force and the induction equation which is the result of combining Maxwell's equations and Ohm's law for a moving, conducting fluid. All of the variables depend on only the x and y coordinates, except the pressure which has a constant gradient p_z in the z -direction. When the coordinates are scaled by the channel half-height a and the variables are normalized, the important equations reduce to two linear, simultaneous partial differential equations in two unknowns:

$$\nabla^2 u + M \frac{\partial B}{\partial x} = -1 \quad (1)$$

$$\nabla^2 B + M \frac{\partial u}{\partial x} = 0, \quad (2)$$

where u and B are the normalized velocity and induced magnetic field,

$$u = \frac{\eta}{a^2 (-p_z)} v_z$$

$$B = \frac{\eta}{a^2 (-p_z)} \frac{1}{\sqrt{\sigma \eta} \mu_0} B_z$$

and

$$\nabla^2 = \frac{\partial^2}{\partial x^2} + \frac{\partial^2}{\partial y^2}.$$

The solutions for the channel made out of insulating material have been found by Shercliff.² Note that the normalized equations (1) and (2) differ from those used by Shercliff. The mechanical constraint imposed on the fluid is that the velocity be zero at the walls; the electrical constraints require that there be no current into the walls, or equivalently that the induced magnetic field assume a constant value (zero) at the walls. The solutions are given in a Master's thesis⁴ and are infinite series of terms; solutions for the normalized velocity u , normalized induced magnetic field B , and average velocity u_0 are given in this report.

$$u(x, y) = \sum_{k=0}^{\infty} \frac{2(-1)^k}{\ell n_k^3} \left[1 + \frac{\sinh m_{2k} \cosh m_{1k} x - \sinh m_{1k} \cosh m_{2k} x}{\sinh (m_{1k} - m_{2k})} \right] \cos n_k y \quad (3)$$

$$B(x, y) = \sum_{k=0}^{\infty} \frac{2(-1)^k}{\ell n_k^3} \left[\frac{\sinh m_{2k} \sinh m_{1k} x - \sinh m_{1k} \sinh m_{2k} x}{\sinh (m_{1k} - m_{2k})} \right] \cos n_k y \quad (4)$$

$$u_0 = \frac{1}{\ell} \int_0^{\ell} \int_0^1 u(x, y) dx dy = \frac{2}{\ell^2} \sum_{k=0}^{\infty} \frac{1}{n_k^4} \left[1 - \frac{N_k (\cosh N_k - \cosh M)}{2n_k^2 \sinh N_k} \right], \quad (5)$$

where

$$m_{1k} = \frac{1}{2} [-M \pm N_k]$$

$$N_k = \sqrt{M^2 + 4n_k^2}$$

$$n_k = \frac{\pi}{2\ell} (2k+1)$$

In order to visualize the velocity, which is an even function of x and y , the contours of u/u_0 in one quarter of the channel have been plotted in Fig. XVI-2 for $\ell = 2.0$ and $M = 0.5$, respectively. In Fig. XVI-3 appear the contours of induced magnetic field, which are lines of current density.

For channels made out of perfectly conducting material, the electrical constraint is that the tangential electric field be zero at the walls, or equivalently that the normal derivative of the induced magnetic vanish at the walls. The solutions for the normalized velocity u , induced magnetic field B , and average velocity u_0 are given here.

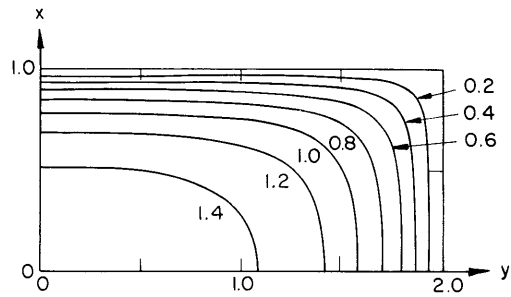


Fig. XVI-2. Normalized velocity contours in insulating walls for $M = 5.0$ and $l = 2.0$.

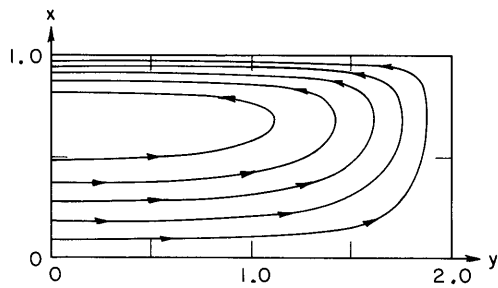


Fig. XVI-3. Contours of induced magnetic field in insulating walls for $M = 5.0$ and $l = 2.0$.

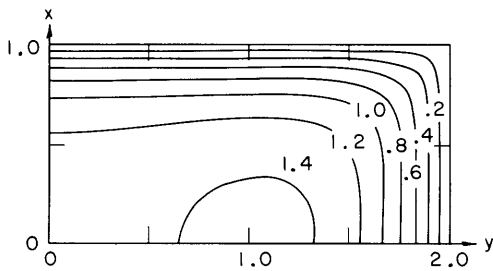


Fig. XVI-4. Normalized velocity contours in perfectly conducting walls for $M = 5.0$ and $l = 2.0$.

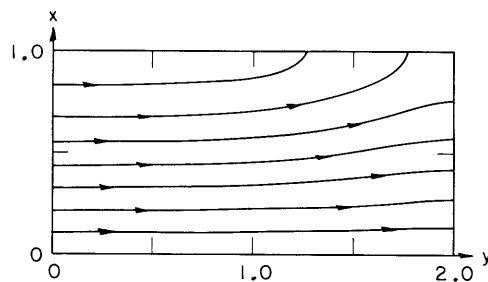


Fig. XVI-5. Contours of induced magnetic field in perfectly conducting walls for $M = 5.0$ and $l = 2.0$.

$$u(x, y) = \sum_{k=0}^{\infty} \frac{2(-1)^k \cos m_k x}{m_k} \frac{1}{m_k^2 + M^2} \left[1 - \frac{a_k E_k(y) - \beta_k F_k(y)}{a_k \sinh 2a_k \ell - \beta_k \sin 2\beta_k \ell} \right] \quad (6)$$

$$B(x, y) = \sum_{k=0}^{\infty} \frac{2(-1)^k \sin m_k x}{m_k} \frac{1}{m_k^2 + M^2} \left[-\frac{M}{m_k} + \frac{a_k F_k(y) + \beta_k E_k(y)}{a_k \sinh 2a_k \ell - \beta_k \sin 2\beta_k \ell} \right] \quad (7)$$

where

$$E_k(y) = \sinh a_k(\ell+y) \cdot \cos \beta_k(\ell-y) + \sinh a_k(\ell-y) \cdot \cos \beta_k(\ell+y)$$

$$F_k(y) = \cosh a_k(\ell+y) \cdot \sin \beta_k(\ell-y) + \cosh a_k(\ell-y) \cdot \sin \beta_k(\ell+y)$$

and

$$u_0 = \sum_{k=0}^{\infty} \frac{2}{m_k} \frac{1}{m_k^2 + M^2} \left[1 - \frac{m_k (\cosh 2a_k \ell - \cos 2\beta_k \ell)}{\ell (m_k^2 + M^2)^{1/2} (a_k \sinh 2a_k \ell - \beta_k \sin 2\beta_k \ell)} \right], \quad (8)$$

where

$$a_k = \sqrt{\frac{m_k}{2}} \sqrt{m_k + \sqrt{m_k^2 + M^2}}$$

$$\beta_k = \sqrt{\frac{m_k}{2}} \sqrt{-m_k + \sqrt{m_k^2 + M^2}}$$

$$m_k = \frac{\pi}{2}(2k+1).$$

These solutions agree with those obtained by Chang and Lundgren,³ except for a factor of 4 in $E_k(y)$ and $F_k(y)$ and a minus sign in Eq. 7. Contour plots like the previous ones are presented in Figs. XVI-4 and XVI-5. The maximum velocity does not occur at the center of the channel, but there are two maxima symmetrically located at $x = 0$ and $y = \pm C$ ($C < \ell$). This phenomenon is more graphically illustrated by Fig. XVI-6, which is an isometric drawing of the velocity profiles in one quarter of a channel made out of perfectly conducting material for $M = 10.0$ and $\ell = 2.0$.

The rectangular channel with perfectly conducting walls parallel to the applied magnetic field and insulating connecting walls is the structure of the MHD conduction generator or pumps. No analytical solutions have been found to satisfy the boundary conditions, but a successive overrelaxation technique may be used to solve the finite difference equations corresponding to Eqs. 1 and 2 with the appropriate boundary conditions. Contour maps of the normalized velocity and induced magnetic field in the open-circuited generator pump are presented in Figs. XVI-7 and XVI-8. With the indicated normalization,

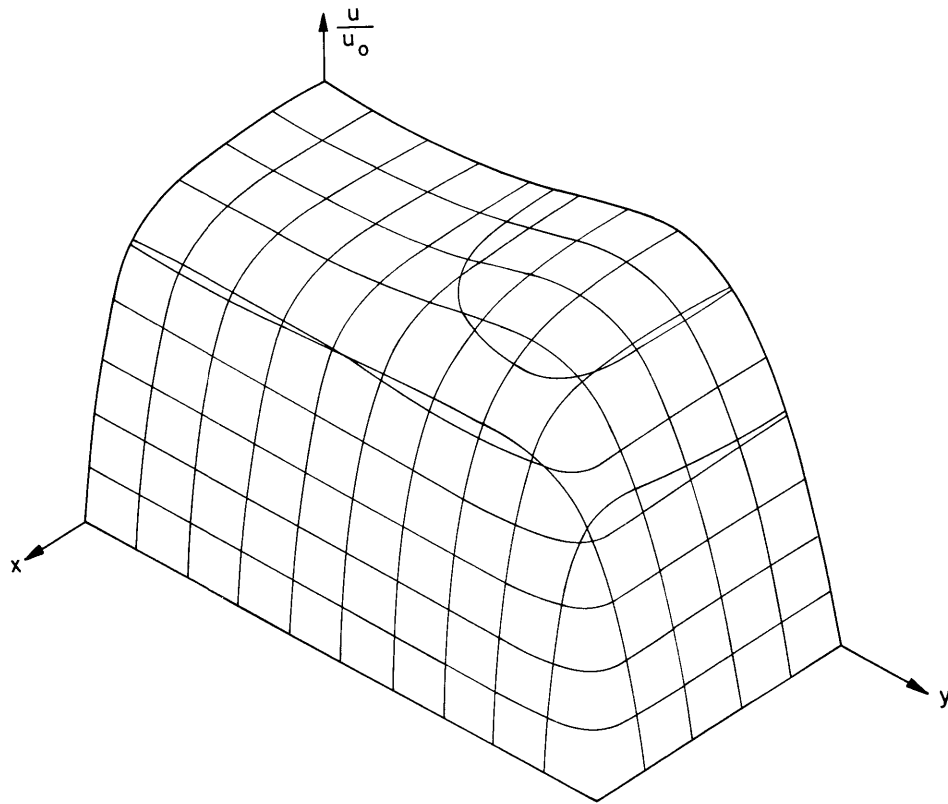


Fig. XVI-6. Isometric of velocity profile in perfectly conducting walls for $M = 10.0$ and $\ell = 2.0$.

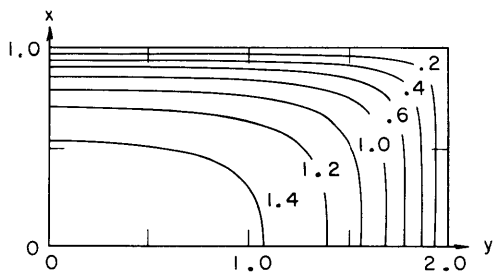


Fig. XVI-7. Normalized velocity contours in open-circuited MHD generator for $M = 5.0$ and $\ell = 2.0$.

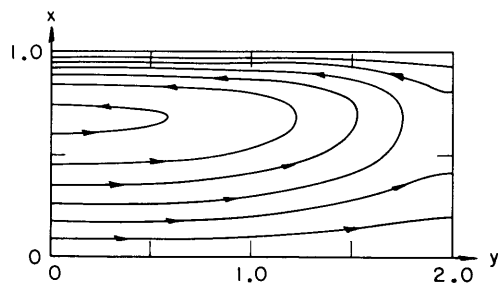


Fig. XVI-8. Contours of induced magnetic field in open-circuited MHD generator for $M = 5.0$ and $\ell = 2.0$.

the velocity contours are valid for any value of the net current through the conducting fluid in the channel, with one exception: For a given pressure gradient and a particular current the fluid can be brought to rest. The effect of the net current flow is more adequately described in the above-mentioned thesis,⁴ and velocity contours of all three sets of boundary conditions and other values of M and l are also included there.

The maxima in the velocity profiles in perfectly conducting walls for Hartmann numbers of 5 and greater indicate that the applied magnetic field has a destabilizing effect on the flow in this case. Calculations are now being extended to higher values of Hartmann numbers.

J. C. Wissmiller, W. D. Jackson

References

1. J. Hartmann, Hg. — Dynamics I, Kgl. Danske Videnskab. Selskab. Math.-fys. Medd., Vol. 15, No. 6 (1937).
2. J. A. Shercliff, Steady motion of conducting fluids in pipes under transverse magnetic fields, Proc. Cambridge Phil. Soc. 49, 136-144 (1953).
3. C. C. Chang and T. S. Lundgren, Duct flow in magnetohydrodynamics, Z. Angew. Math. Phys. 12, 100-114 (1961).
4. J. C. Wissmiller, Velocity Profiles for Magnetohydrodynamic Flows in Rectangular Ducts, S.M. Thesis, Department of Electrical Engineering, M. I. T., 1964.

B. MAGNETOHYDRODYNAMIC POWER GENERATION WITH LIQUID METALS

Cycle studies of the liquid-metal MHD system made with a condensing ejector have indicated that favorable cycle efficiencies are associated with high performance or efficient operation of the condensing ejector. For reference purposes a schematic

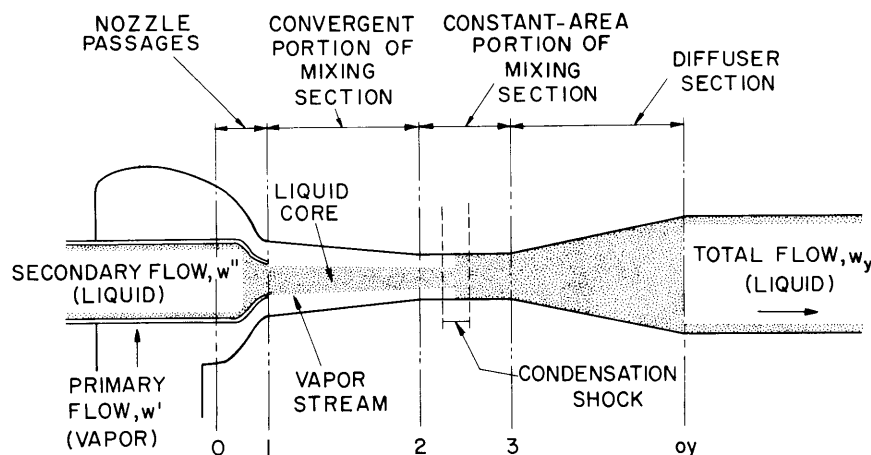


Fig. XVI-9. Illustrating the geometry and processes of the condensing ejector.

(XVI. PLASMA MAGNETOHYDRODYNAMICS)

diagram of the condensing ejector is presented in Fig. XVI-9. High-performance operation usually accompanies the existence of one or more of the following conditions:

1. The exit stagnation pressure, p_{oy} , is significantly higher than both inlet stagnation pressures, p'_o and p''_o .

2. The flow rate ratio, w , is low, with

$$w = w''/w'. \quad (1)$$

3. The vapor velocity at section 1, V'_1 , is high, generally in the high subsonic or supersonic range.

4. The contraction ratio, A_1/A_2 , is high. Note that for the geometry shown in Fig. XVI-9, a maximum value for the contraction ratio can be defined as

$$\left(\frac{A_1}{A_2}\right)_{\max} = \frac{A'_1 + A''_1}{A''_1} = \frac{1 + X}{X}, \quad (2)$$

where A'_1 and A''_1 are the flow areas occupied by the vapor and liquid streams, respectively, at the inlet to the mixing section, and X , the inlet area ratio, is defined as

$$X = \frac{A''_1}{A'_1}. \quad (3)$$

The performance of the condensing ejector can be judged quantitatively by the use of an efficiency based on the availability concept of Keenan.¹ Such an efficiency might be defined as

$$\eta = \omega \frac{(h_{oy} - h''_o) - T''_o(S_{oy} - S''_o)}{(h'_o - h_{oy}) - T''_o(S'_o - S_{oy})}. \quad (4)$$

The numerator in Eq. 4 represents the minimum shaft power required to take the liquid between the two states in question, while the denominator represents the maximum shaft power available from the vapor stream between the two states indicated.

The available experimental data^{2,3} show maximum efficiencies of approximately 40 per cent. The experimental conditions, however, were not selected so as to obtain maximum efficiency. The data reported elsewhere² were obtained at fairly high inlet vapor velocity, but the flow-rate ratios were too high and the contraction ratios too low for high efficiency performance. The data of Miguel and Brown³ were obtained at high contraction ratios, but the inlet vapor velocities were too low and the flow-rate ratios were too high for high efficiency performance. These data did, however, confirm the performance analysis presented previously^{2,4} over a wide range of variables.

The performance analysis was used to determine operating conditions for

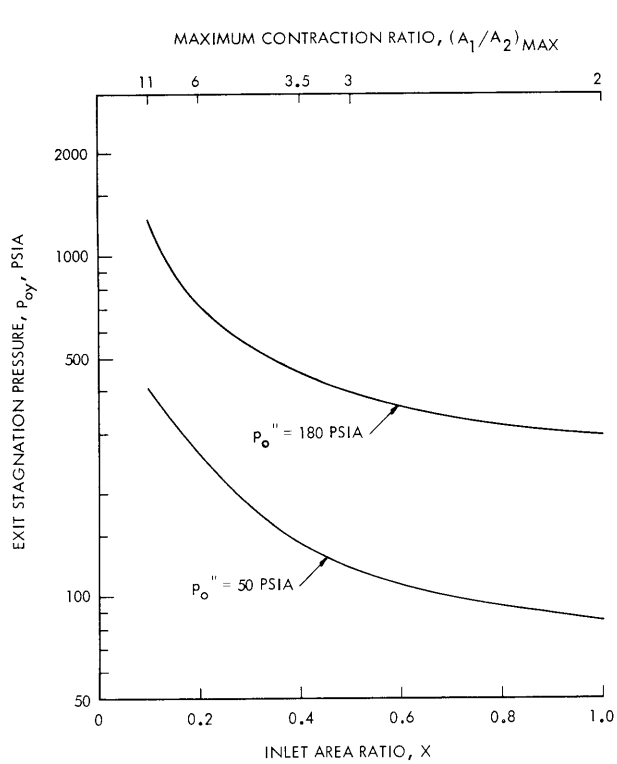


Fig. XVI-10. Effect of inlet area ratio on exit stagnation pressure.

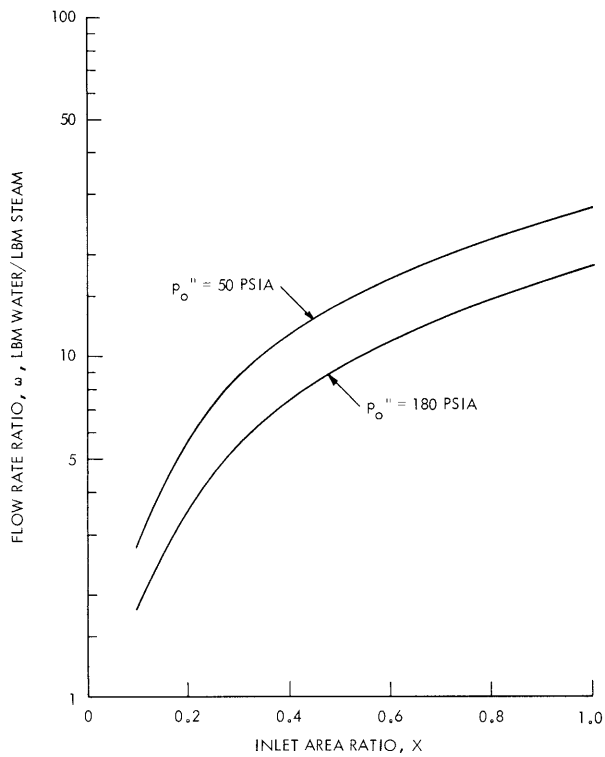


Fig. XVI-11. Effect of inlet area ratio on flow rate ratio.

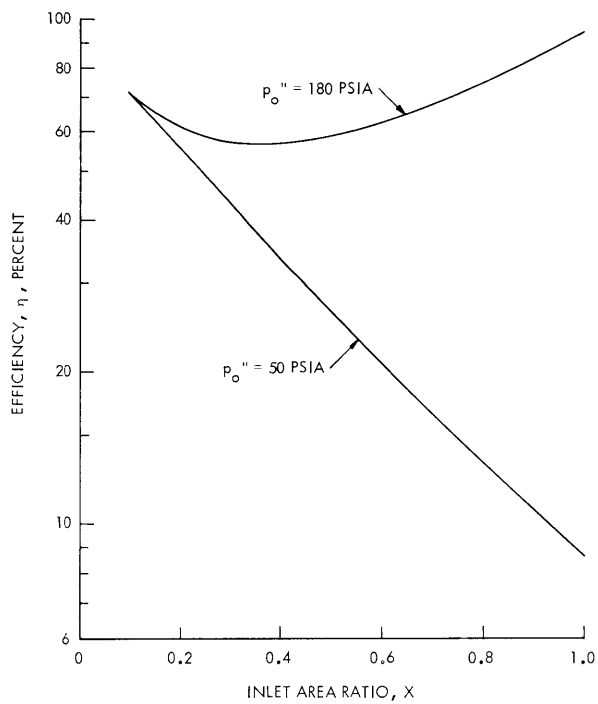


Fig. XVI-12. Effect of inlet area ratio on efficiency.

(XVI. PLASMA MAGNETOHYDRODYNAMICS)

high-performance testing of the condensing ejector by using available steam supplies in the Engineering Projects Laboratory at M. I. T. The results of these calculations are shown in Figs. XVI-10 through XVI-12. In addition to the variables listed on these graphs the following assumptions were used.

Working fluids: steam and water

$$p'_0 = p''_0$$

t'_0 = saturation temperature at p'_0

$$t''_0 = 40 \text{ F}$$

p_1 selected to make V'_1 correspond to sonic velocity

A_1/A_2 given by Eq. 2.

Figure XVI-10 indicates that appreciable exit stagnation pressures can be expected, even when using steam and water at 50 psia if the inlet area ratio is low and hence the contraction ratio high. The flow-rate ratios are low and the efficiencies are high as shown in Figs. XVI-11 and XVI-12, respectively, at these same values of inlet area ratio. One must be careful in the interpretation of these results, since as the inlet area ratio is reduced two effects are encountered. First, if the flow rate is too low, then the flow at sections 3 and 4 will not be in a liquid state. This assumption was used in the performance analysis and is always checked in the calculations. Second, conditions will be calculated for which the efficiency is 100 per cent. This should correspond to reversible adiabatic or isentropic operation of the condensing ejector. Although conditions that correspond to actual operation in a reversible manner can be found, such conditions have not been assumed for these calculations. There remains as one of the major questions, "How reversibly can the condensing ejector be made to operate?"

The results shown in Figs. XVI-10, XVI-11, and XVI-12 are being used to design a research condensing ejector test facility. It is planned to use steam and water pressures as indicated. The inlet area ratio and contraction ratio will also be varied over the range of interest with strong attention paid to the small values of inlet area ratio. The mixing section shapes will be designed with the available mixing section analysis for some design points in the high-efficiency operating range.

G. A. Brown

References

1. J. H. Keenan, Availability and irreversibility in thermodynamics, Brit. J. Appl. Phys. 2, 183-192 (1951).
2. G. A. Brown, An Analysis of NUOS Condensator Test Data with a New Theory for the Variable Area Condensator, Report No. 44, Joseph Kaye and Company, Inc., Cambridge, Massachusetts, 1961.

(XVI. PLASMA MAGNETOHYDRODYNAMICS)

3. J. Miguel and G. A. Brown, An Analytical and Experimental Investigation of a Condensing Ejector with a Condensable Vapor, AIAA Paper 64-469, July 1964.
4. G. A. Brown, A Summary of Research on Two-Phase Flow in Nozzles and in the Condensing Ejector, Report 8040-2, Engineering Projects Laboratory, Department of Mechanical Engineering, M. I. T., 1964.

C. EXPERIMENTAL MEASUREMENTS OF THE THERMAL CONDUCTIVITY OF CESIUM VAPOR

The primary purpose of this project was to measure the thermal conductivity of cesium vapor. The data would be used to predict other transport properties of cesium, as well as properties of the other alkali metals. These metals have recently become important in various energy-conversion and heat-transfer processes. A small amount of experimental data and theoretical estimates of the properties of the alkali metals have been published.¹⁻⁵ It is expected that the method which was developed for this project, as applied to cesium, could be adapted to the other alkali-metal vapors, as well as to other gases.

One of the problems in working with the alkali metals is their incompatibility with many engineering substances, because of chemical reactions. This precludes the use of glass and the precious metals for the range of pressures and temperatures that we must have so that the mean-free path will be small compared with the apparatus dimensions. Standard techniques⁶⁻⁹ for measuring the thermal conductivities of gases and vapors take advantage of the low thermal emissivities of the precious metals to minimize the simultaneous thermal radiation that must accompany a temperature difference across a vapor-filled space. Generally the gases for which the results of thermal conductivity measurements have been reported are electrically nonconducting. This is requisite for the hot-wire-cell method (one of the standard methods) to be easily used. Since the alkali metals are easily ionized and the condensed vapor on the surface of an insulator serves to short-circuit the hot-wire and give erroneous readings, the hot-wire-cell method is not suitable for alkali metals unless special precautions are taken.

Previous work¹⁰⁻¹² with the same goal as ours provided the basis for this work. The apparatus employed in this experiment consists of a pair of cells containing the test gas. The gas space in each cell is an annular region between concentric cylinders. Although the lengths and inner diameters of these gas spaces are the same for both cells, the outer diameters are unequal. The temperatures of the outer cylinders of both cells are maintained equal by placing them in the same oven. The temperatures of the inner cylinders are maintained equal to a higher level by separate resistance heaters located

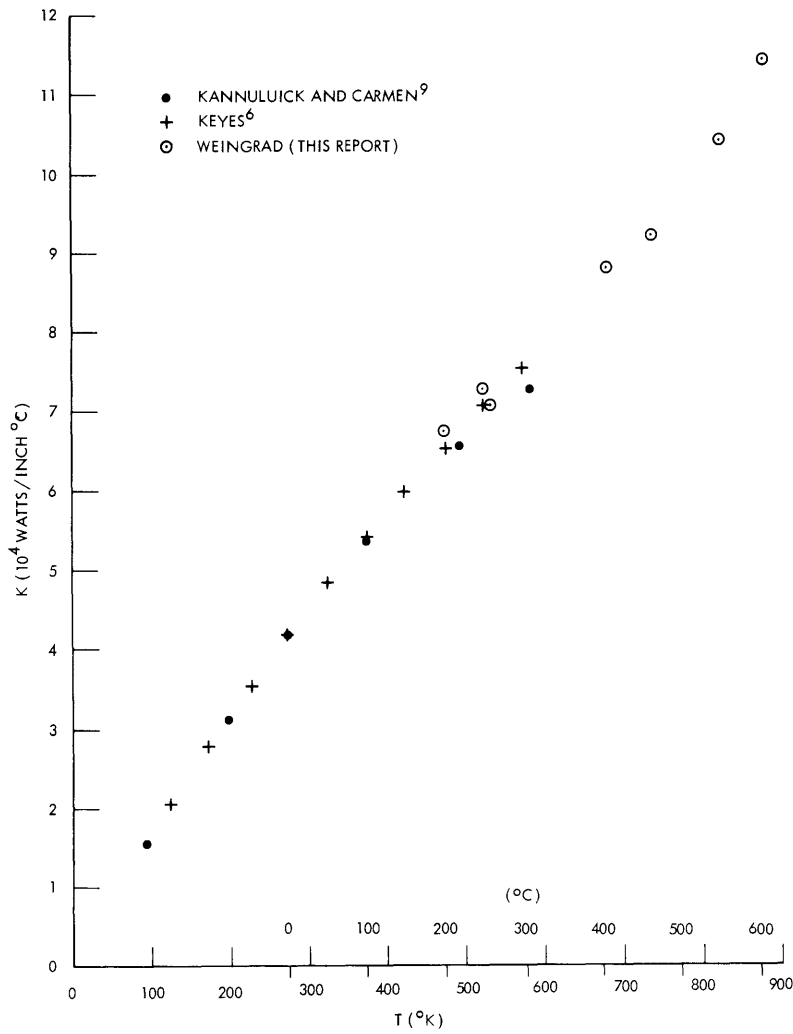


Fig. XVI-13.
 Experimental values of the thermal conductivity coefficient of argon vs temperature.

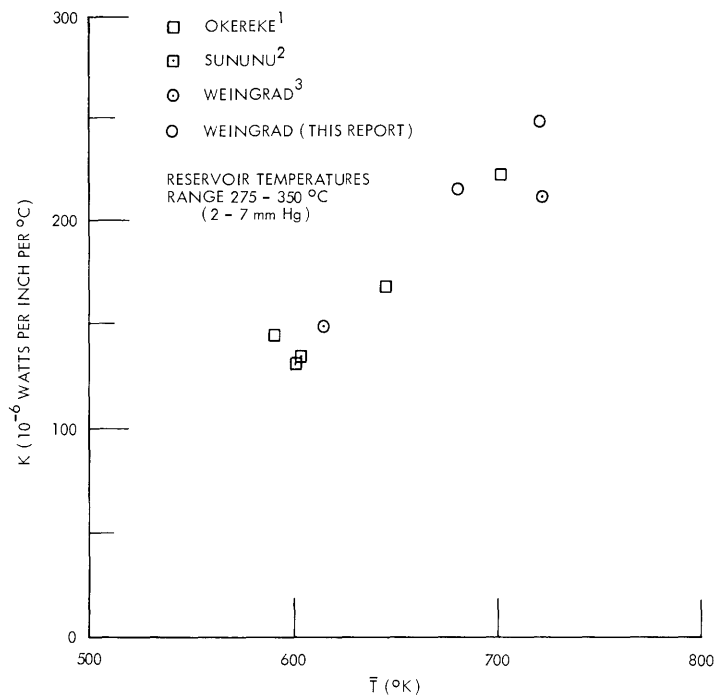


Fig. XVI-14.
 Experimental values of the thermal conductivity coefficient of cesium vapor vs temperature.

(XVI. PLASMA MAGNETOHYDRODYNAMICS)

along the center line of each cell. Since the heat transfer through the gas depends on the magnitude of the annular spacing (which differs for these cells), the two heaters will require unequal power inputs to attain the condition of equal temperature of the inner cylinders. Assuming that the heat transfer by radiation and by conduction through the solids is equal for both cells, we may determine the thermal conductivity from measurements of the power inputs and the cell dimensions. A detailed description of these assumptions and calculations has been presented in the author's thesis.¹²

The thermal conductivity of argon was measured first in order to check the accuracy of the apparatus. From the results shown in Fig. XVI-13 it is concluded that the accuracy is entirely satisfactory.

Early failure of the apparatus limited the cesium measurements to two temperatures, 680°K and 720°K, the conductivities being 215 and 249 microwatts/inch °C, respectively. These measurements were obtained from one cell only because the second did not function properly after it was charged with cesium. Although this prevented us from using the comparative method described here, the results were in general agreement with previous data (Fig. XVI-14). A compilation of data obtained by our group is included in Fig. XVI-14.

J. Weingrad

References

1. H. E. Weatherford, R. M. Tyler, and K. Ku, Properties of Inorganic Energy-Conversion and Heat-Transfer Fluids for Space Applications, WADD-TR-61-96, November 1961.
2. I. Granet, Some Selected Properties of Cesium, *J. Am. Soc. Naval Engineers* 72, 319 (1960).
3. M. Gottlieb and R. J. Zollweg, Thermal conductivity of cesium vapor, *Advanced Energy Conversion* 3, 37 (1963).
4. W. R. Martini, Theoretical calculation of the thermal conductivity of cesium vapor at thermionic temperatures, *Advanced Energy Conversion* 3, 49 (1963).
5. S. Kitrilakis and M. Meeker, Experimental determination of the heat conduction of cesium gas, *Advanced Energy Conversion*, 3, 59 (1963).
6. F. G. Keyes, Heat Conductivity, Viscosity, Specific Heat and Prandtl Numbers for Thirteen Gases, Project SQUID TR-No. 37, Massachusetts Institute of Technology and Princeton University, April 1, 1952.
7. Proceedings of 2nd Biennial Gas Dynamics Symposium, Northwestern University Press, Evanston, Illinois, 1958.
8. R. D. Present, Kinetic Theory of Gases (McGraw-Hill Book Company, New York, 1958).
9. W. Kannuluick and E. Carmen, *Proc. Phys. Soc. (London)* 65B, 701 (1952).
10. S. A. Okereke, An Experimental Measurement of the Thermal Conductivity of Cesium Vapor, S.B. Thesis, Department of Mechanical Engineering, M.I.T., 1963.

(XVI. PLASMA MAGNETOHYDRODYNAMICS)

11. J. H. Sununu, An Experimental Measurement of the Thermal Conductivity of Cesium Vapor, S. M. Thesis, Department of Mechanical Engineering, M. I. T., 1962.

12. J. Weingrad, Thermal Conductivity Measurements of Cesium Vapor, S. B. Thesis, Department of Mechanical Engineering, M. I. T., 1963.

D. PREDICTION OF MAGNETOHYDRODYNAMIC INDUCTION GENERATOR PERFORMANCE

In this report we discuss the MHD induction machine in terms of attainable over-all efficiency. Weight and cost considerations are not included. Attention is directed toward the generator, since the success of liquid-metal power generation systems is critically dependent upon the development of efficient generators. In contrast, the efficiency of MHD pumps is not necessarily the most important factor in selecting operating conditions. The absence of rotating components and seals is the primary advantage of these pumps, and the power levels at which they are usually operated do not, as a practical matter, make the minimization of losses an important design objective.

The induction generator, in principle, may be used in both open- and closed-cycle power systems. In the former, combustion gases serve as the working fluid, in the latter, either a plasma or a liquid metal may be used. It has been shown that the plasma conductivity attainable within the limits imposed by heat-source temperatures is too low for reasonable power factors and power densities.^{1,2} Our discussion, accordingly, is limited to liquid-metal generators.

1. Optimum Operating Regime

First, the conditions required to attain an efficiency of over 70 per cent for the generator and associated equipment are reviewed. The limiting electric efficiency in terms of the fluid slip s , $\frac{1}{1-s}$, must be much higher to allow for other losses. This constrains s to lie in the range $-\frac{1}{4} \leq s < 0$, but it should not be too close to zero to avoid excessive losses resulting from the fluid velocity profile³ and finite machine length.^{4,5}

The circulating power should be small compared with the real power for small excitation and capacitive losses, and this requires the magnetic Reynolds number R_M to be ~ 10 . Another requirement is that sR_M be approximately or greater than unity to attain a power density of the same value as the corresponding DC machine. Another consideration is that low sR_M values lead to less output power for the same excitation losses, and accordingly to lower efficiency. This criterion cannot always be satisfied, as R_M is limited by attainable fluid properties, but the total efficiency decreases as R_M becomes smaller and the entry length increases for a finite-length machine.

The value of α should be small (0.1 or less) to keep the power density high. It is limited by the minimum value of the channel half-width set by construction problems.

For an air-core machine the power density is decreased for the same exciting current because of the increased reluctance of the magnetic circuit. For $a = 0.1$ the power level is less than 1/10 of its iron-core value.⁶ As the iron-core generator must be carefully designed to yield an only marginally acceptable efficiency, the air-core machine is inherently not capable of meeting the required performance, and will not be considered here. It may be of interest only when weight or temperature limitations rule out iron.

The velocity profile for a slit-channel machine may significantly decrease the efficiency for small s . For laminar flow and s around -0.1 , the Hartmann number M based on the rms magnetic field must be much greater than 50 to prevent a 5 or 10 per cent decrease in the efficiency. This condition is automatically satisfied for a high power density. For turbulent flow the boundary-layer analysis shows that a slight loss in the efficiency is encountered even for M in the range 500-1000. The non slit-channel machine is not considered here, because of its low power level and severe profile effects.

Finally, the dimensions of the machine are restricted by end and edge considerations. The machine must be several wavelengths long so that the finite length does not decrease the power level. A decrease in the power level represents a decrease in the over-all efficiency because less output power is obtained for the same viscous and excitation losses. The machine width should be larger than the wavelength to keep edge losses small. The wavelength cannot be too small, or $a \leq 0.1$ cannot be satisfied.

2. High-Power Generator

A design for a generator producing an output power in the 100-megawatt range will be discussed. This is not an optimum design, and is not chosen to meet any specifications, but it does give an idea of attainable efficiencies and the limits on machine parameters. The results are summarized in Table XVI-1.

Eutectic sodium potassium (NaK), 78 per cent potassium by weight, is chosen for the fluid. The fluid used for an actual machine will depend on thermodynamic considerations, which are not considered here. The fluid temperature will be high because of the heat source and losses. The properties⁷ of NaK at 700°C are:

$$\begin{aligned}\sigma &= 1.1 \times 10^6 \text{ mhos/m,} \\ \eta &= 1.5 \times 10^{-5} \text{ kg/m-sec,} \\ \rho &= 7.1 \times 10^2 \text{ kg/m}^3.\end{aligned}$$

The dimensionless parameters are chosen to be $s = -0.1$ for a high limiting efficiency, $R_M = 10$ so that $|sR_M| = 1$, and $a = 0.1$ for a high power density. For an iron-core machine the relative permeability is large, and is taken to be infinite except when finding the core loss. The magnetic Reynolds number cannot be increased without increasing the relative viscous loss. If we make $|s|$ smaller, we run into three

Table XVI-1. High-power generator designs.

Parameter	Definition	Units	1	2	3	4
s	$(v_s - v)/v_s$		-0.1			
R_M	$\mu\sigma v_s/k$		10			
a	ak		0.1			
$\omega/2\pi$	frequency	cps	60			
v_s	field velocity	m/sec	52.3			
v	fluid velocity	m/sec	57.5			
a	channel half-height	m	0.0139			
c	channel width	m	2			
λ	wavelength	m	0.871			
k	$2\pi/\lambda$	1/m	7.21			
ℓ	machine length	m	8.71	17.4	8.71	17.4
R_e	Reynolds number		1.49×10^7			
NI		amp-turns/m	10^5		$\sqrt{2} \times 10^5$	
$ B $		wb/m ²	0.889		1.26	
M	Hartmann number		747		1050	
P_s		megawatts	47.3	105.	94.6	209.
P_m		megawatts	55.0	120.	108.	237.
e_g - Limit		per cent	86.0	86.9	87.3	88.2
P_e		megawatts	0.80	1.60	1.13	2.26
P_{cap}		megawatts	0.95	2.09	1.89	4.18
P_v		megawatts	4.47	8.94	4.47	8.94
P_{in}		megawatts	59.5	129.	113.	246.
P_{out}		megawatts	45.6	101.	91.6	203.
e_g - Total		per cent	76.6	78.0	81.2	82.4
Δp		psi	2699	5860	5120	11200

difficulties: the power density drops because R_M is fixed, the profile losses become larger, and the penetration length of the field increases. The ratio α cannot be decreased because the gap between the exciting plates is already less than 1 per cent of the length or width of the plates, and construction is difficult. This choice of machine parameters, dictated by the nature of the interaction, automatically leads to a high-power machine. It is necessary to move away from this optimum to lower the power level, and the result is a lower efficiency.

Since the choice of machine parameters is inter-related, only the frequency or wavelength, c , and the exciting surface current amplitude NI remain. For example,

$$v_s = \frac{\omega}{2\pi} \lambda, \quad (1)$$

and, for NaK,

$$R_M = 0.22 \frac{\omega}{2\pi} \lambda^2. \quad (2)$$

Choosing $\frac{\omega}{2\pi}$ to be 60 cps gives 0.871 m and 52.3 m/sec, respectively, for λ and v_s . Increasing $\frac{\omega}{2\pi}$ while holding either R_M or λ constant increases v_s , and makes the performance worse because the viscous loss increases faster than the output power. Increasing R_M without increasing v_s is desirable but leads to lower frequencies. Increasing $\frac{\omega}{2\pi}$ and holding v_s constant has the disadvantage of reducing R_M . These considerations probably rule out higher frequencies. For the remaining dimensions, the machine is made 10 wavelengths long and 2 m wide to minimize end and edge effects. Note that α is very small compared with both ℓ and c .

The final parameter, the surface current amplitude, should be large for a high power level, but not so large that the iron saturates. Choosing $NI = 10^5$ amp-turns/m gives 0.899 wb/m^2 for the flux density, low enough so that the iron teeth between the slots where the coils are located should not saturate.

At this point, the limiting efficiency, including profile and end effects, is calculated before the other losses are added. First, $R_e = 1.49 \times 10^7$, so that the flow will probably be turbulent. Turbulent boundary-layer theory can be used to determine the changes in the powers resulting from the varying velocity across the channel. The power transferred to the exciting winding P_s is unchanged, but the mechanical power P_m is multiplied by the profile factor $F_m = 1.038$. The mechanical power is increased because of circulating currents.⁸

Finite length is included by means of the ratios of P_s and P_m for finite-to-infinite-length machines. The values of 0.827 and 0.842, respectively, are obtained for these parameters.^{4,5} The efficiency is decreased, since the ratio is less for P_s than P_m , and the over-all efficiency is further decreased because the power output is less for the same viscous and coil losses. The end and profile factors are independent for a slit

(XVI. PLASMA MAGNETOHYDRODYNAMICS)

channel. Using the profile and finite-length factors gives an output electrical power P_s of 47.3 megawatts, an input mechanical power P_m of 55 megawatts, and an efficiency of 86 per cent without inclusion of the other losses.

The coil, capacitor, core, and viscous losses must still be taken into account. The coil loss is calculated from the conductor volume and the conductivity. For the assumed NI, by using a current density of 10^4 amps/in.² and copper at 200°C, the coil loss P_e is 0.80 megawatt. A temperature of 200°C is selected because the coils and core must be considerably cooler than the fluid so that the magnetic properties of the core are retained.

Capacitors are required for power-factor correction with the induction generator. This might be supplied by conventional synchronous generators in a large system, but allowance is made here on the basis of the loss attributable to the static capacitors for a self-contained system. The power loss is determined by the Q of the capacitors plus the associated lead loss. For conventional power-system capacitors, the best obtainable, at present, is a Q of around 300 at 60 cps. A total Q of 50 is assumed to include losses in the leads plus the additional capacitance required to balance the normally inductive generator load. The capacitor power loss P_{cap} is 0.95 megawatt, since the real and reactive powers are equal for $|sR_M| = 1$. An increased Q will cause at most a 2 per cent increase in efficiency.

The core loss depends on the core construction. A solid core is not acceptable, and a laminated core must be used as in conventional machinery to reduce the circulating currents and loss. The core loss is found as a function of the field strength and the lamination thickness from experimental measurements of the power loss per pound, including both I^2R and hysteresis losses. For calculation purposes, the magnetic flux density in the core is assumed to be constant for a skin depth and zero elsewhere, in the manner used to calculate the power loss in conductors with skin depth. For a high-grade transformer steel the approximate core loss is 0.033 megawatt, an amount that may be neglected.

The calculation of the viscous power loss is complicated by the lack of experimental information on MHD turbulent flows. The friction factor is not known, and the use of a friction factor to calculate the viscous loss in MHD flows gives up to twice the correct loss, because of the nonuniform electromagnetic force.⁹ Three possible figures are available for the friction factor, the ordinary hydrodynamic results, Harris's result which includes both viscous and circulating-current losses, and a theoretical calculation for MHD flows by using boundary-layer theory.¹⁰ The difference between the three is less than the factor $\frac{1}{2}$ in the viscous power, so that the ordinary hydrodynamic value is used without the factor $\frac{1}{2}$. This gives 4.47 megawatts for P_v , which is 10 per cent of the output power, and is the largest of the losses. Note that P_v is proportional to v^3 , while P_s is proportional to v with constant R_M , so that increasing v will make the

net performance worse.

Based on these approximate results for the losses, the total power output is 45.6 megawatts, and the total efficiency is 77 per cent.

The three other high-power designs of Table XVI-1 show the increased efficiency resulting from increasing the length and NI. Only the revised figures are entered in the table. Doubling the length, design 2, increases the ratios of P_s and P_m for finite to infinite-length machines to 0.913 and 0.920. This gives a slightly higher power level relative to the losses and better efficiency.

In designs 3 and 4, NI is increased by $\sqrt{2}$, which doubles the power level. This decreases the profile factor F_m to 1.022 because of the increased M. The efficiency is higher because the power output is increased for the same viscous loss, and because F_m is smaller. Ideally, NI should be further increased, but this is not practical because of saturation. Already $B = 1.26 \text{ wb/m}^2$, which may be too large for the teeth. Evidently, the generator should be operated at maximum magnetic field for highest efficiency.

To complete the calculations, the total pressure difference across the machine and the coil resistance are found for the first design. The pressure difference, $\frac{P_{in}}{(2acv)}$, is 2699 psi or 184 atmospheres, including the viscous pressure drop. This is large but not excessive for the powers considered. It could be decreased by departing from the uniform-channel generator. If the width increases along the machine, the velocity drops and some of the dynamic head of the flow may be utilized.

3. Medium-Power Generator

A slightly different procedure is used for a generator with an output power around 1 megawatt because operation at the optimum point is no longer possible. Instead, certain dimensions, set by the reduced volume, and the magnetic field are specified. It has been shown that operation at the highest possible magnetic field, limited only by core saturation, is best because the power output increases faster than the losses. The magnitude of the field is specified as 1 wb/m^2 , probably large enough for saturation in the teeth.

The generator volume is reduced to produce a more compact machine and to reduce the viscous and excitation losses along with the output power. The minimum wavelength is limited to $\sim 1/3 \text{ m}$ by construction difficulties at these power levels and to keep R_M reasonably large. Here, λ and c are chosen as $\frac{1}{2} \text{ m}$ each, and the machine length as 4 wavelengths. This leads to increased end and edge effects, but appears to be unavoidable. The values $\alpha = 0.1$ and $\frac{\omega}{2\pi} = 60 \text{ cps}$ are again used, and NaK is retained as the fluid. Higher frequencies give poorer results, as we have mentioned. For this design $v_s = 30 \text{ m/sec}$, $R_M = 3.3$, and $M = 482$.

The only unspecified parameter is s . Three designs showing the effect of varying

Table XVI-2. Medium-power generator designs.

Parameter	Units	1	2	3
s		-0.1	-0.2	-0.3
R_M		3.3		
a		0.1		
$\omega/2\pi$	cps	60		
v_s	m/sec	30		
v	m/sec	33	36	39
a	m	0.00796		
c	m	0.5		
λ	m	0.5		
k	1/m	12.6		
l	m	2		
R_e		4.82×10^6	5.25×10^6	5.69×10^6
NI	amp-turns/m	0.838×10^5	0.953×10^5	1.12×10^5
$ B $	wb/m ²	1		
M		482		
P_s	megawatts	0.429	1.17	1.97
P_m	megawatts	0.592	1.53	2.71
e_g - Limit	per cent	72.5	76.1	72.7
P_e	megawatts	0.038	0.044	0.051
P_{cap}	megawatts	0.0086	0.023	0.039
P_v	megawatts	0.059	0.075	0.095
P_{in}	megawatts	0.65	1.61	2.80
P_{out}	megawatts	0.38	1.10	1.88
e_g - Total	per cent	58.7	68.4	67.1
Δp	psi	359	814	1310

(XVI. PLASMA MAGNETOHYDRODYNAMICS)

s at constant magnetic field are given in Table XVI-2. The exciting current is increased with increasing s to hold the magnetic field constant, because of the larger reaction field. The ratios of P_s and P_m for a finite-to-infinite-length machine and the profile factors F_m are listed in Table XVI-3 for $s = -0.1, -0.2,$ and -0.3 . The efficiency before adding the other losses goes through a peak around $s = -0.2$. This is due primarily to the finite-length effect, which increases with smaller $|s|$. F_m also increases, but not as rapidly until $|s|$ becomes still smaller. This shows the limitation on s and the efficiency; the efficiency cannot be made arbitrarily large as in the ideal model.

Table XVI-3. End and profile factors for medium-power generators.

Factor		$s = -0.1$	-0.2	-0.3
End	P_s	0.5451	0.7404	0.8333
	P_m	0.6564	0.7925	0.8667
Profile	$\frac{\delta^*}{a}$	0.00722	0.00762	0.00799
	F_m	1.040	1.023	1.017

The power dissipations in the exciting winding, capacitors, and fluid viscosity are calculated as in section 2, and the core loss is assumed to be negligible. The value of P_v is less than 10 per cent of P_m , and the percentage decreases with increasing $|s|$.

The total efficiency is lowest for $s = -0.1$ and climbs to a more reasonable figure with increasing $|s|$. There is a peak, probably around $s = -0.24$. The peak total efficiency occurs at a higher slip than the peak limiting efficiency because the additional losses do not increase as fast as the electromagnetic powers. The efficiencies, both limiting and total, are less than those for the high-power machine, because of the lower R_M and increased end losses. For small R_M the end effect for a short machine increases; thus a short machine with reasonable efficiency is impossible. This rules out decreasing λ because the increased number of wavelengths in the machine is at least partially offset by the smaller R_M and increased end effect.

E. S. Pierson, W. D. Jackson

References

1. W. D. Jackson, E. S. Pierson, and R. P. Porter, Design Considerations for MHD Induction Generators, International Symposium on Magnetohydrodynamic Electrical Power Generation, Paris, July 6-11, 1964.
2. E. S. Pierson, The MHD Induction Machine, Sc.D. Thesis, Department of Electrical Engineering, M. I. T., Cambridge, Massachusetts, 1964, Section 7.3.

(XVI. PLASMA MAGNETOHYDRODYNAMICS)

3. Ibid., Chapters 4 and 5.
4. Ibid., Chapter 6.
5. E. S. Pierson and W. D. Jackson, Magnetohydrodynamic induction machine of finite length, Quarterly Progress Report No. 75, Research Laboratory of Electronics, M.I.T., October 15, 1964, pp. 92-103.
6. E. S. Pierson, Sc.D. thesis, op. cit., Section 3.3.
7. C. B. Jackson (Editor-in-Chief), Liquid Metals Handbook - Sodium (NaK) Supplement, U.S. Atomic Energy Commission and the Bureau of Ships, United States Navy, 1956.
8. E. S. Pierson, Sc.D. thesis, op. cit., Chapter 5, Section 7.3, and Appendix D.
9. Ibid., Appendix D.
10. Ibid., Chapter 5.